The DOI for this manuscript is doi:
10.1175/2009JTECHA1303.1

Joint Calibration of Multi-Platform Altimeter Measurements of Wind Speed and Wave Height Over the Past 20 Years

S. Zieger *, J. Vinoth and I. R. Young

Faculty of Engineering & Industrial Sciences, Swinburne University of Technology

* *Corresponding author address:* Swinburne University of Technology, Faculty of Engineering & Industrial Sciences, PO Box 218 (H38), Hawthorn, Victoria, 3122, Australia.

E-mail: szieger@swin.edu.au

ABSTRACT

Since 1985 – for more than 23 years, seven altimeter missions have provided global coverage of significant wave height and wind speed. This study undertakes a long term analysis of the accuracy and stability of altimeter derived values of significant wave height and wind speed from the satellites: ERS1, ERS2, ENVISAT, GEOSAT, GEOSAT Follow-On (GFO), JASON1 and TOPEX. The study is a necessary step in developing a quality controlled and fully calibrated/validated dataset from the combined satellites. Calibration of all altimeters is performed against NODC buoy data over the extended period. These calibrations are validated using intercomparisons between satellite missions at cross-over ground points. This analysis shows that for a number of the satellites, small "step-like" changes occur during the missions. These inconsistencies are removed by sub-dividing these missions and undertaking a partial calibration for each section of the mission. The analysis also highlights that care is necessary when attempting to apply relationships between radar cross-section and wind speed derived for one altimeter to other platforms. Before undertaking such steps it is first necessary to apply a platform specific radar cross-section offset to the data.

1. Introduction

Many oceanographic applications require the compilation of long-term databases of accurate oceanic properties (in the present case, significant wave height H_s and wind speed U_{10}). Historically, such wave climate data is gathered through the deployment of oceanographic buoys and more recently though the use of numerical models (Caires et al. 2004). Both approaches have significant deficiencies. In situ buoy data has obvious limitations in terms of geographical and temporal coverage and the expense of deploying and maintaining such systems. Model data clearly solves these limitations, but relies critically on the accuracy of the model. Even though present day models contain sophisticated representations of wind-wave physics, the accuracy of such models is still limited (Tolman 2002). Studies by e.g. Dobson et al. (1987) and Monaldo (1988) have shown that active remote sensing satellites, particular Ku-band radar altimeter systems, are capable of measuring significant wave height (H_s) and wind speed (U_{10}) to an accuracy comparable to in situ observations (e.g. buoys).

Since the launch of GEOSAT in 1985, a total of seven independent altimeter missions (cf. 2b) have been operational, potentially providing a unique database with global coverage spanning more than two decades. Once calibrated and quality controlled, such a database could be an invaluable tool for many oceanographic applications, such as:

- measurement of changes in global wind and wave climate
- development of methods to determinate extreme values
- investigation of extreme meteorological systems (i.e. hurricanes)

To date, however, these independent data sources have not been compiled to form one single, long term database. Although some attempts have been made to form datasets from combined altimeter missions (e.g. Cotton and Carter 1994; Callahan et al. 1994; Young 1999a; Alves and Young 2003), a comprehensive database of the type proposed has not previously been developed. Furthermore, procedures to process data gathered by polar orbiting altimeter satellites are still relatively underdeveloped. The future of oceanography will inextricably move towards satellite observations of the ocean, supported by in situ point instruments for data calibration.

This paper describes the development of such a database, including the validation, calibration and quality control of the data set. The arrangement of the paper is as follows. Section 2 describes both the buoy and altimeter data sources used. Section 3 provides details of the quality control and calibration/validation of the altimeter data. Calibrated results for wind speed and wave height are given within the subsections. Finally, the conclusions of the study are considered in Section 4 which provides a tabular summary of the final calibrated results for wind speed and wave height.

2. Data Sources

National Oceanographic Data Center (NODC) buoy data was used to provide in situ data for a uniform calibration (ground truthing) for all altimeter missions over the entire period (described below). The satellite data (Geophysical Data Records GDRs) were sourced from the respective agencies and separately compiled for each available radar altimeter up to 2008, covering the historic satellite platforms GEOSAT, ERS1, and TOPEX and the ongoing missions ENVISAT, ERS2, GFO, and JASON1. Note that the TOPEX/POSEIDON mission included three separate altimeter instruments: TOPEX side A (cycles 1–235), side B (cycles 236–481), and the POSEIDON altimeter. The POSEIDON altimeter has not been considered in this paper as its data is co-incident with TOPEX.

a. Buoy data

Wind and wave data were downloaded from the NOAA Marine Environmental Buoy Database, maintained by the NODC. The data archive contains records from various stations (e.g. lighthouses, oil platforms, and buoys, etc.) reporting a range of environmental parameters (e.g. air temperature, sea temperature, wind speed, wave height, wave direction, etc.) in constant time intervals (Evans et al. 2003). Despite the lack of spatial coverage this archive features an excellent temporal coverage back to the early seventies. For the present purposes, only moored buoys were processed.

<< Fig. 1, p. 40 (MapNODCBuoyLocation.eps) >>

The buoy data format (F291) contains nine different types of data records (e.g. nondirectional wave spectra, subsurface temperature/salinity, subsurface current, etc.). In the present analysis, only header and environmental data records were processed [NODC (cited 2008)]. In addition to geographic location and date/time, values of significant wave height, wind speed, air/sea temperature, and anemometer height were extracted from the environmental data records. The NODC moored buoy network consists of various platform types ranging from 3 m, 6 m, 10 m, to 12 metre discus buoys (Meindl and Hamilton 1992). Large discus buoys were deployed in areas of harsh climate, such as the Bering Sea and due to maintenance services and refurbishing procedures, all buoys are subjected to changes in their location with time (Meindl and Hamilton 1992). For calibration purposes the database consists of 195 different stations, distributed over 619 locations. The locations of the buoys are shown in Figure 1, highlighting the restricted geographical distribution of data, with the vast majority of the locations being near continental North America and almost exclusively confined to the Northern hemisphere.

Each buoy type collects wind speed at a different height (anemometer height). Therefore a height based correction was applied to provide compatibility between buoy observations and altimeter estimated wind speeds at 10 metres (U_{10}) above the mean sea surface. Following Young (1999b) and assuming a logarithmic marine boundary layer, the records were corrected to 10 m reference height U_{10} using the relationship:

$$U_{10} \; = \; u \sqrt{\kappa^2/C_d}\, ln^{-1}(z/z_o) \tag{1}$$

where u is the wind speed measured at a height z above sea level, z_o is the surface roughness length, κ is the von Kármán constant and C_d the drag coefficient. The drag coefficient varies with both wind speed and sea state (Young 1999b). However, field measurements of C_d typically scatter over an order of magnitude. Noting this, and the inherent inaccuracies associated with floating buoy measurements of wind speed (see later this section), a constant value of C_d was used. For the present application, a representative value of $C_d = 1.5 \times 10^{-3}$ was adopted and with the von Kármán constant $\kappa = 0.4$, (5.11) from Young (1999b) can be solved to yield $z_o = 3.271 \times 10^{-4}$ m. This value of z_o is consistent with the relationship developed by Donelan (1990) $z_o/H_{rms} = 5.53 \times 10^{-4}(U_{10}/C_p)^{2.66}$, where C_p is the phase speed of the waves and H_{rms} is the root mean squared wave height. Typical open ocean values of $U_{10}/C_p \approx 1$ and $H_{rms} \approx 0.8$ m yield results comparable to $z_o = 3.271 \times 10^{-4}$ m.

The buoy-network transmits hourly observations via the Geostationary Operational Environmental Satellite (GOES) system to the data acquisition center (Hamilton 1986). Some care needs to be exercised in interpreting the logging cycles for the buoys, which have changed over the extended period being considered. Typically, the buoys record wind speed averaged over a period of 8 minutes and the significant wave height from a time series of duration 20 minutes. On occasions, however, the significant wave height was determined from a 40 minute time series. The 20 minute wave records typically commence 20 minutes past the hour and the wind records commence 42 minutes past the hour. On a small number of occasions, the wave records commenced 30 minutes past the hour (i.e. both wind and wave records conclude at 50 minutes past the hour). When 40 minute wave records were employed, these records commenced on the hour. Records recorded after 5 May 1992, typically recorded the observation time as 50 minutes past the hour (i.e. the time when wind and wave records concluded). Prior to this date, the recording time was stored as the closest whole hour (i.e. the next hour for records concluding at 50 minutes past the hour) (personal communication, NODC). For the present analysis, the times associated with wind and wave records were corrected to the centre of the respective time series.

In the present analysis, buoy data is used as the reference or "ground truth". However, such data is not free of error, as it is limited by both sampling variability (i.e. the respective time series are just one realisation of the process) (Bendat and Piersol 1971) and instrumental accuracy. Floating buoys are subject to systematic bias. At low wind speeds, the rocking motion of the buoy will "pump" the anemometer resulting in an overestimation of wind speed. Conversely, at high wind speed/wave height, sheltering by wave crests will result in an underestimation of the wind speed. Buoy accuracies are specified as 1.0 m s^{-1} for wind speed and 0.2 m for significant wave height [NDBC (cited 2008)].

b. *Altimeter Data*

Spaceborne Radar altimeters have observed the oceans for more than two decades. Figure 2 shows the various missions over this period. As can be seen, there is an almost continuous record since 1985. The Radar altimeter can be used to estimates several oceanographic parameters over a footprint ranging between 1 and 10 km in diameter (Chelton et al. 2001). The precise size of a pulse-limited footprint depends on range, pulse width, and wave height itself (Chelton et al. 2001). The footprint for GEOSAT is approximately 5 km (Cheney et al. 1987), ERS1, ERS2 and ENVISAT are 7 km, TOPEX, JASON1 are 6 km (Queffeulou 2004) and GFO is approximately 3 km (Walker 1995).

<< Fig. 2, p. 41 (FigTemporalCoverageAlti.eps) >>

The altimeter estimates significant wave height (H_s) from the sea surface variance (σ^2) which is characterized by the slope of the leading edge of the returned waveform (Chelton et al. 2001; Holthuijsen 2007). The significant wave height is defined as $H_s = 4\sqrt{\sigma^2}$, where σ^2 is the variance of the sea surface elevation (Chelton et al. 2001). Wind speed (U_{10}) is related to the backscatter coefficient (σ_o) representing the ratio of the power scattered back to the altimeter from the illuminated surface to the incident power (Chelton et al. 2001). For small incident angles the radar cross-section, σ_o, can be inversely related to the surface wind speed (Brown et al. 1981; Goldhirsh and Dobson 1985; Chelton and Wentz 1986; Witter and Chelton 1991; Young 1993; Freilich and Challenor 1994; Young and Holland 1996; Chelton et al. 2001; Abdalla 2007). Typically, altimeter measurements of H_s have smaller error than for U_{10} when compared with buoy measurements and the accuracy (rms error) has been stated as within 0.5 m for H_s and 1.8-2.0 m s^{-1} for U_{10}. For TOPEX altimeter measurements, Kshatriya et al. (2001) state smaller values of 0.3 m and 1.6 m s^{-1}, respectively.

Data for each of the seven satellites was obtained, as detailed in Table 1. The details of the orbit geometry (i.e. repeat cycle and inclination angle) is different for each satellite. All systems were, however, placed in polar orbits providing global coverage, the period of data available being shown in Figure 2. As indicated in the table, in each case Geophysical Data Records (GDRs) have been used for the analysis. This is important as calibration values and data quality often varies between different altimeter data products.

<< Table 1 (p. 33) >>

3. Quality Control and Validation/Calibration Methods

a. Altimeter Quality Control

Geophysical Data Records (GDRs) are not free from errors and a visual examination of such data clearly shows data "spikes" (see Figure 3). Such erroneous data often occurs at the land/sea boundary, in the proximity of islands or over sea ice. In compiling a large database it is important that such erroneous data is removed in a reliable fashion, whilst not discarding reliable data. In a similar fashion to that proposed by Young and Holland (1996), a three-pass quality control process was applied to the data.

Pass 1

The GDRs contain data which enables an initial quality assessment. The first pass focussed on the H_s data and flagged data which met any of the following criteria as erroneous:

- If $H_s > 30$m the data point was flagged as erroneous.
- Most data sets contain a flag which indicates whether the data point is over ocean or land/ice, based on a land/sea mask. All points identified as over land/ice were flagged as erroneous.
- GDRs typically provide an observation approximately once per second. Each one second value is the average of between 10 and 20 waveforms, depending on the satellite. Waveforms which do not meet pre-defined parameters are discarded. If the final number of waveforms averaged falls significantly below the maximum possible (10 or 20), then this is an indication that the data is of questionable quality. The number of waveforms averaged for each point is typically recorded within the GDR. If the number of averaged waveforms was less than 75 % of the maximum number, the data was flagged as erroneous.

Pass 2

The data from Pass 1 was divided into blocks of 25 points. Such blocks represent approximately 180km along the ground track. This distance was considered large enough to obtain a representative group of observations (25 in this case), but not so long that there would be significant variability within the block due to geophysical processes (different wind systems etc.). A number of different block sizes were tested before adopting this value.

- Individual values in the block were flagged as erroneous if $\frac{|H_s - \bar{H}_s(block)|}{\sigma_{H_s}(block)} > 2$ where $\bar{H}_s(block)$ is the mean of the points in the block and $\sigma_{H_s}(block)$ is the standard deviation of the block.

Pass 3

In the final pass, blocks identified in Pass 2 were further considered. These blocks were re-divided into sub-blocks, either side of flagged points. These sub-blocks were further considered.

- each sub-block was examined for outliers, as in Pass 2, with any further points failing the test flagged as erroneous.
- If the ratio $R = \frac{\sigma_{H_s}(block)}{\bar{H}_s(block)}$ is large, then it indicates that it is possible that there are multiple "spikes" in the block. Therefore, if $R > 0.5$ the entire sub-block was discarded.

<< Fig. 3, p. 42 (MapGFODespike.eps) >>

Figure 3 shows an example of a typical satellite pass with the raw GDR data (gray) and the quality controlled data (solid lines) shown. The ascending ground track is shown as a smooth line (left panel) with recorded wave height (H_s) and wind speed (U_{10}) along the ground track as a function of latitude (right panel). The most southern section of the track passes over the Antarctic continent towards the Southern Ocean. Due to the Southern Hemisphere Winter erroneous data below 60° S can be linked to sea ice. At approximately

30° S data “spikes” occur due to the transition from water to the Australian continent, whilst the effects of islands are shown between 20° S and 10° N when the satellite passes over Indonesia. Further north, valid data is shown, as the satellite passes over a typhoon in the Philippine Sea (30° N) measuring wave heights of 9 m and wind speeds up to 20 m s^{-1}. As the track continues (40° N), it passes over the Kamtschatka Peninsula and finally enters open waters moving towards the Arctic Ocean. As shown in this figure, the quality assurance algorithm successfully flags erroneous data whilst not discarding quality observations, even in areas where there are strong spatial gradients of wind speed and/or wave height.

Over the full duration of each of the satellite mission, the quality control procedure removed inappropriate data records amounting to: 15.5 % for GEOSAT, 9.6 % for ERS1, 8.1 % for ERS2, 4.7 % for TOPEX, 9.0 % for GFO, 8.4 % for JASON1, and 17.1 % for ENVISAT.

b. Altimeter Calibration

Calibration of the altimeter data was carried out by comparing buoy measurements with quasi-simultaneous radar observations for both significant wave height (H_s) and wind speed (U_{10}). In the case of altimeter wind speed a single wind speed model relating wind speed to radar cross-section (σ_o), applicable to all altimeter platforms was determined (see below, this section). Comparisons between buoy and satellite altimeter data require criteria for the spatial and temporal separation between such observations to be adopted. Following Dobson et al. (1987); Monaldo (1988); Gower (1996); Queffeulou (2003, 2004); Queffeulou et al. (2004) these limits were set at 50 km and 30 min respectively. Since buoy data was largely reported hourly (Hamilton 1986), the largest temporal separation is 30 min, and following Monaldo (1988) such a time separation leads to an expected uncertainty of 0.5 m s^{-1} for wind speed and 0.3 m for significant wave height.

Along-track averages were calculated for all matching transects (maximum 100 km, i.e. ± 50 km, assuming there is no land over the 100 km) and time tags of each altimeter overpass were linear interpolated to the two nearest hourly buoy records for H_s and U_{10} respectively. The 50 km spatial separation criteria defines a circle of diameter 100 km in which data is considered. A transect which passes directly over the buoy will have a transect length of 100 km. More distant passes will define shorter chords of the circle. Only transects with greater than 4 valid points were considered, so as to ensure statistically stable values. In order to ensure that the point buoy measurements and the spatially averaged altimeter data are comparable, it is desirable not to consider data recorded close to land, where there may be strong spatial gradients of wave height or wind speed. Therefore, buoy stations within 40 km of land were not considered in the calibration process (Dobson et al. 1987).

Dobson et al. (1987) and Monaldo (1988) analysed typical errors associated with altimeter-buoy comparisons, considering spatial and temporal separation, buoy record duration and altimeter footprint averaging size, as well as platform-specific instrumental error. Monaldo concluded that differences for H_s and U_{10} of approximately 0.4 m and 1.8 m s^{-1} respectively, can be expected, when comparing altimeter and buoy estimates, whereas Dobson et al. determined that an overall rms uncertainty for H_s and U_{10} of 0.5 m and 1.8 m s^{-1}, respectively, may be expected using collocated measurements within a 50 km range.

Collocated buoy-altimeter measurements were compared using linear regression analysis. Since both variables (buoy and altimeter) have measurement uncertainty associated with them, a traditional regression analysis is not appropriate (Stoffelen 1998). Rather, a reduced major axis regression (RMA) was used to estimate the best-fit between the two measurements (Trauth 2007). RMA regression is applicable when errors in both quantities need to be considered. The RMA methodology minimizes the triangular area between the data point and the regression line (Trauth 2007). Mayor outliers were eliminated prior to application of the RMA analysis. This was achieved by applying a robust regression algorithm and eliminating data points with low weighting. Robust regression is an iteratively re-weighted least squares analysis (O'Leary 1990).

<< Fig. 4, p. 43 (FigScatterEnvisatBuoy.eps) >>

Figure 4 illustrates a typical calibration result, for JASON1 altimeter data. Clearly observable is the significantly higher scatter for U_{10} than for H_s. Note, that scatter plots for all other satellites look similar and therefore are not shown. The resulting RMA analyses for all satellites are however given in Table 3.

To evaluate the suitability of the final regression analysis, the following statistical parameters were evaluated: root mean square error, $RMSE$ (Eq. 2), mean absolute error, MAE (Eq. 3), Pearson's correlation coefficient, ρ (Eq. 4), the number of sample points and the number of outliers.

$$
\begin{aligned}
RMSE: \quad \epsilon &= \sqrt{\frac{1}{n}\sum^{n}(\hat{y}-y)^2} \qquad (2)\\
MAE: \quad e &= \frac{1}{n}\sum^{n} \mid \hat{y}-y \mid \qquad (3)\\
\rho(Y,\hat{Y}) &= \frac{Cov(Y,\hat{Y})}{\sqrt{Cov(Y,Y)Cov(\hat{Y},\hat{Y})}} \qquad (4)
\end{aligned}
$$

In Equations (2)-(4), the hat separates the estimate (calibrated value) from the reference measurement (buoy observation) and Cov is the covariance between two random variables. The values of y take on either H_s or U_{10} and the upper case values refer to vectors.

Although the RMA analysis can be performed directly for values of H_s, its application for U_{10} firstly requires the adoption of an appropriate wind speed algorithm relating U_{10} and the radar cross-section, σ_o. A wide range of such wind speed algorithms have been published. In general one can distinguish between one- and two-parameter wind speed models (Fig. 5). Amongst others, Monaldo and Dobson (1989) and Gourrion et al. (2002) investigated the enhancement of wind speed estimates by adding significant wave height as an additional parameter in the wind speed function. A comprehensive summary of wind speed algorithms (incl. equations) can be found in Young (1993) and Young and Holland (1996). In this analysis, all major wind speed algorithms including: Brown et al. (1981); Chelton and McCabe (1985); Chelton and Wentz (1986); Goldhirsh and Dobson (1985); Witter and Chelton (1991); Freilich and Challenor (1994); as well as the recent models from Gourrion et al. (2002) and Abdalla (2007) were compared with NODC buoy measurements, and validated for performance using RMS error estimates from Eq. (2). Published wind speed algorithms were typically derived for one particular altimeter platform (e.g. for SEASAT as in Chelton and McCabe 1985), thus the possibility of a platform related bias (c.f. Table 2) has to be considered before applying a uniform wind speed model to the data from multiple altimeter missions. With the present data set, it would be possible to develop and fit an optimal functional form to the combined data set of $U_{10} - \sigma_o$ values. As the many existing functions are, however, very similar, as shown in Figure 5, such a process was not attempted. Comparisons with available data did, however, show that there were clear σ_o offsets between the data sets and when applying an algorithm to a satellite for which it was not derived, the offset needs to be considered. The rms error (ϵ) between the wind speed model and in situ buoy measurements was minimized by selecting the optimal offset for the radar cross section σ_o. The resulting values are shown in Table 2. These offset values need to firstly be applied before a specific algorithm can be applied to a specific satellite data set. It is clear that the bulk of the available data in Figure 5 is concentrated between 4 m s^{-1} and 10 m s^{-1}. In order to ensure the algorithm fit is not biased to this region, data was averaged into 5 cm s^{-1} bins and these average values used in the optimization.

<< Table 2 (p. 34) >>

It remains unclear if sea-state dependence, particular significant wave height (H_s), should be considered. Although this was the subject of previous research, e.g. Monaldo and Dobson (1989); Glazman and Greysukh (1993) and Gourrion et al. (2002), results differ. As stated by Monaldo and Dobson, significant wave height potentially affects the physical link between σ_o and surface wind speed in two ways. First, the local wave heights are the combination of waves which propagate into the area and wind waves generated by local wind fields. Second, the presence of waves may affect the development of short waves on the surface, which influence the radar cross-section. Distinguishing such affects within the scatter of the data is challenging, as seen in Figure 5. The error analysis in Table 2 shows no clear reduction in RMS error with the inclusion of H_s as an additional parameter. For these reasons, two-parameter functions involving H_s have not been considered further in this analysis.

<< Fig. 5, p. 44 (FigTopexWindSpeedAlg.eps) >>

Based on error statistics from Eq. (2) to (4) the model proposed by Abdalla (2007) was selected as the default wind speed algorithm for the database and is briefly described below. Abdalla investigated the relationship between surface wind speed, as obtained from the numerical wind model of the European Centre for Medium-Range Weather Forecasting (ECMWF) and Ku-band altimeter backscatter coefficients from ENVISAT. The resulting algorithm was derived from two months (January – February 2005) of collocation data containing approximately 163,000 samples. Finally, the algorithm was verified against model wind speed for ENVISAT (two years), JASON1 (18 months), and ERS2 (five years) altimeter measurements. Abdalla adopted a two branch approach to estimate a first-guess wind speed (U_m) by fitting linear and exponential segments for lower and higher radar cross section (σ_o) respectively (cf. Eq. (5)).

$$U_m = \begin{cases} 46.5 - 3.6 \cdot \sigma_o & \text{for} \quad \sigma_o \leq 10.917 \text{ dB} \\ 1690 \cdot exp(-0.5 \cdot \sigma_o) & \text{for} \quad \sigma_o > 10.917 \text{ dB} \end{cases} \tag{5}$$

Fine-tuning was carried out to ensure that model wind speeds matched buoy observations, with U_m from Eq. (5) adjusted to:

$$U_{10} = U_m + 1.4 \cdot U_m^{0.096} \cdot exp(-0.32 \cdot U_m^{0.096}) \quad (6)$$

In Eq. (5) and (6) wind speed values have units of [m s^{-1}] and Radar cross-section has units of [dB]. Since 24 October 2005, equations (5) and (6) have been used operationally for the ENVISAT radar altimeter (Abdalla 2007).

As the Abdalla (2007) relationship was derived for data with $U_{10} < 18\,\mathrm{m\ s}^{-1}$, a modified form of the Young (1993) high wind speed relationship was adopted for $U_{10} > 18\,\mathrm{m\ s}^{-1}$. The offset in Eq. (7) was modified, such that it intercepts the Abdalla (2007) result at $18\,\mathrm{m\ s}^{-1}$.

$$U_{10} = -6.4 \cdot \sigma_o + 69, \text{ if Eq. (6)} > 18 \text{ m s}^{-1} \quad (7)$$

In Eq. (7) U_{10} has units of [m s^{-1}] and σ_o has units of [dB]. Although the error statistics supported the adoption of the Abdalla (2007) algorithm as the preferred wind speed model, a visual inspection of Table 2 shows that the widely applied Witter and Chelton (1991) algorithm also performs well.

With an appropriate wind speed algorithm adopted, it is possible to carry out the calibrations of both H_s and U_{10} for each of the altimeters. Table 3 provides the RMA derived calibration results for each of satellites. The results shown represent the average over the entire period of operation for each satellite mission and utilize all co-located buoy observations over that period. In addition, a subset of published altimeter calibration models is also shown for comparison purposes.

<< Table 3 (p. 35) >>

Queffeulou (2003) adopted a very similar calibration approach (averaging altimeter transect within 50 km radius and 30 min temporal separation) to that proposed here, but based on a shorter database. As can be seen from Table 3 the present results are in good agreement with Queffeulou (2003) for H_s across all satellite missions. Young (1999a) used a database of 10 years duration, but compared monthly means within 4° by 4° bins, rather than co-located passes. This different methodology appears to give rise to measurable differences in the calibration results.

For GEOSAT H_s, Dobson et al. (1987) proposed that the altimeter is generally 0.40 m lower than buoy observations ($\epsilon = 0.49\,\mathrm{m}$, $\mathrm{e} = 0.36\,\mathrm{m}$ and $\mathrm{n} = 116$). Carter et al. (1992) provided evidence for a GEOSAT scaling error with altimeter values being 13 % lower than buoy values. However, ordinary least square regression, not forced through the origin, leads to $H_s^* = 1.093\,H_s + 0.116$ ($\mathrm{n} = 164$), where H_s^* is the corrected significant wave height (Carter et al. (1992)), which is in good agreement with the result presented here.

Ray and Beckley (2003) correlated TOPEX and JASON1 significant wave height with buoy observations and concluded that for TOPEX, $H_s^* = 1.046\,H_s - 0.070$ ($\epsilon = 0.17\,\mathrm{m}$, $\rho = 0.985$ and $\mathrm{n} = 399$) and for JASON1, $H_s^* = 1.100\,H_s - 0.104$ ($\epsilon = 0.21\,\mathrm{m}$, $\rho = 0.983$ and $\mathrm{n} = 368$). The TOPEX result is in excellent agreement with the present result, which uses approximately ten times the amount of data. The JASON1 result differs slightly from the present result with a larger slope but more negative offset.

For wind speed, it is not possible to directly compare the results with previous calibrations. In the present analysis, the Abdalla (2007) wind speed algorithm was adopted for all satellites, but with a σ_o offset for each satellite chosen so as to reduce the RMS error. The resulting values of altimeter wind speed were then further calibrated against co-located buoy wind speed using the RMA analysis. Not surprisingly, the results all have regression slopes near 1.00 and small offsets.

c. Altimeter Collocation Analysis

For much of the period under consideration (since 1993), multiple altimeter missions have been in orbit. As a result, it is possible to cross-validate instrument performance against other platforms, by comparing observations at cross-over points. Ground-track crossovers between simultaneously operating altimeter platforms were considered when both platforms passed the same ground point within 30 min. In contrast to Queffeulou (2004), 100 km (50 km each side) along-track averages were compared, rather than the closest 1-s measurements. As for the buoy comparisons, the spatial average provides a more statistically stable comparison than a single point observation. For all platforms, a valid ground-track contains at least ten individual 1-s altimeter data points for averaging. The altimeter cross-over analysis was not used to calibrate individual platforms, this process being undertaken with the buoy analysis (cf. Section 3b). Rather, scatter plots comparing different altimeters at cross-over points were used as independent validation of the calibrated results. In other words, the cross-over analysis was used as a quality control and validation measure.

<< Fig. 6, p. 45 (MapEnvisatERS2Collocation.eps) >>

Figure 6 shows an example of the spatial coverage of cross-over points for the overlap period of JASON1 and ERS2. In comparison to the buoy calibration process, the very much larger number of co-locations is clear. Figure 7 shows the resulting wave height and wind speed scatter plots for this same case. For all combinations of coincident satellite missions, the calibrated satellite altimeters produced consistent results (RMA regression slope close to 1:1), when averaged over the full durations of co-incident operation.

<< Fig. 7, p. 46 (FigScatterEnvisatERS2.eps) >>

d. Long Term Monitoring

The calibrations performed against buoy data (Table 3) considered all available data for the period of operation of each satellite. As a result, the calibrations are averages over the full satellite missions. It is important to ensure that the calibrations do not vary over the duration of the extended mission. This could be determined by examining differences between buoy and altimeter data as a function of time. A further possibility is to examine differences between co-incident altimeter missions as a function of time at cross-over points. Due to the very much larger data sets for altimeter cross-over points, this second option proved more reliable, with a greater capability in identifying small changes in instrument performance.

Figure 8 shows an example of the differences between TOPEX and ERS2 values of H_s. Due to the large number of observations, data points shown in the plot were thinned using block averages over n points (values of n are given in figure captions, e.g. 20/1 for a 20 point blocked average). If significant discontinuities or data drifts were determined, the data sets were partitioned and a reduced major axis regression was applied for each section of mission. For consistency, the partitioned RMA regression was performed against buoy data, the cross-over analysis acting as an independent quality control. For wind speed measurements, the previously determined, satellite specific, σ_o offsets were retained, any further departures from buoy measurements be corrected using the partitioned RMA analysis. Once the partitioned RMA analysis had been applied, the satellite cross-over plots were examined to ensure the process had removed any inconsistencies between the data sets.

<< Fig. 8, p. 47 (FigTopexDrifCorrection.eps) >>

The most obvious example of a time-specific variation in altimeter performance is the TOPEX drift in H_s which commenced at approximately cycles 163–170 and continues to cycle 235 (April 1997 to January 1999), previously investigated by Challenor and Cotton (1999) and Queffeulou (2004). Challenor and Cotton applied a linear trend model to buoy measurements to remove the drift, whereas Queffeulou fitted a third order polynomial using ERS2 as the reference data set. As illustrated in Figure 8 the drift can be well approximated by an exponential power function of the form:

$$f(t) \;=\; 0.0542 \cdot [\exp(0.0027t)]^{1.1080} - 0.0303 \qquad (8)$$

where the dependent variable t is time, measured in days from 25 April 1997 and $f(t)$ has units of [m]. The correction is valid until 30 January 1999 (0 days $\leq t <$ 645 days). Figure 8 also shows the results once TOPEX data has been corrected using Eq. (8).

<< Fig. 9, p. 48 (FigTopexDrifCorrectionBuoys.eps) >>

Figure 9 shows the difference between TOPEX and buoy H_s, following the removal of the drift. In both cases, Eq. (8) successfully corrects the data. The reduction in available data in Figure 8 since June 2003, is a result of an onboard storage failure on ERS2, which has limited available data from this satellite to locations in the Northern Hemisphere close to receiving stations. This feature is also apparent in Fig. 6.

<< Fig. 10, p. 49 (FigERS1Discontinuities.eps) >>

Changes in altimeter calibration for either U_{10} or H_s were identified for ERS1, ERS2, GFO and TOPEX using this process. Figure 10 shows differences between buoy and ERS1 H_s and U_{10} for the duration of the ERS1 mission. As explained above, changes to calibration were actually identified using altimeter cross-over comparisons. The partial re-calibration was then performed against buoy data and checked using cross-over comparisons. As no single pair of altimeters covers the full ERS1 mission, the buoy comparison is used here for illustrative purposes. The period between 1. January 1994 and 18. February 1995 clearly shows slightly low values of H_s. To correct this effect, the full ERS1 mission was divided into three sections and the partial RMA analysis applied to each section. The panels to the right of Figure 10 show the corrected results, with the offset removed.

<< Fig. 11, p. 50 (FigGFODiscontinuities.eps) >>

Figure 11 shows a similar plot for GFO. Here, discontinuities in U_{10} in the periods before 21. December 2000 and after 21. January 2007 are clear. Again, the partial RMA analysis successfully accounted for these anomalies.

The source of these inconsistencies is unclear and may result from changes to onboard systems, different software implementations etc. Although the long term differences are relatively small (generally less than 1 m s^{-1} in wind speed and 0.2 m in wave height), the value of a long term data base of this type requires confidence in the long term stability of the data.

In the case of TOPEX, the altimeter was changed from the Side-A instrument to Side-B in February 1999. The data did not show a measurable discontinuity at this point, nor any clear degradation in the quality of the Side-A data leading up to the change. This result is consistent with the Side-B calibration study reported by Dorandeu (1999).

The final calibrations for all satellites are provided in Table 4, which details the calibration results applicable in various periods for each satellite, as well as error statistics.

4. Conclusion

The data and procedures outlined here present a detailed analysis of the historic altimeter data base of H_s and U_{10} over the more than 2 decades for which data is available. The process developed calibrates the altimeter records against buoy data and then independently validates these results against independent altimeter missions at cross-over points of ground tracks. The value of such a data set is in that it covers an extremely long duration with global coverage. As such, it is critical that altimeter calibration is stable over this extended duration. This analysis investigates the long term stability of the altimeter missions and concludes that long-term drift of results is generally not an issues (with the exception of TOPEX H_s). However, a number of the missions do exhibit apparent step changes in calibration at various times. Although these changes are not large, they do impact the overall quality and reliability of the data set. These changes in calibration can, however, be corrected by partitioning the data sets with time and independently calibrating the altimeter in each partitioned segment. The reason for these step changes in calibration does not appear to have been well documented and is presumably the result of changes in the software/hardware of the satellite or of processing methods.

A number of relations between the radar cross section and wind speed were investigated and the Abdalla (2007) relationship was ultimately adopted for use with all altimeters. However, the analysis clearly shows that before applying such a relationship across all altimeters, a platform dependent offset must be applied.

Consistent with previous studies, altimeter values of H_s exhibit greater accuracy than U_{10}. Following calibration, the accuracy of the various altimeters are similar, with the rms error being less than 0.25 m for H_s and 1.7 m s^{-1} for U_{10}.

In this study no attempt has been made to look at long-term trends in the final "calibrated" dataset. This is an involved task which requires a careful analysis of the data. The present dataset does, however, provide a unique resource for such studies and this is the subject of ongoing research.

<< Table 4 (p. 36) >>

REFERENCES

Abdalla, S., 2007: Ku-band Radar Altimeter Surface Wind Speed Algorithm. *Envisat Symposium 2007*, European Centre for Medium-Range Weather Forecasts, UK.

Alves, J. H. G. M. and I. R. Young, 2003: On estimating extreme wave heights using combined Geosat, Topex/Poseidon and ERS-1 altimeter data. *Appl. Ocean. Res.*, **25 (4)**, 167–186, doi:10.1016/j.apor.2004.01.002.

Bendat, J. S. and A. G. Piersol, 1971: *Random Data: Analysis & Measurement Procedures*. Wiley-Interscience, 407 pp.

Brown, G., H. Stanley, and N. Roy, 1981: The wind-speed measurement capability of spaceborne radar altimeters. *IEEE J. Ocean. Eng.*, **6 (2)**, 59–63.

Caires, S., A. Sterl, J. R. Bidlot, N. Graham, and V. Swail, 2004: Intercomparison of Different Wind–Wave Reanalyses. *J. Clim.*, **17 (10)**, 1893–1913.

Callahan, P. S., C. S. Morris, and S. V. Hsiao, 1994: Comparison of TOPEX/POSEIDON sigma0 and significant wave height distributions to Geosat. *J. Geophys. Res.*, **99 (12)**, 25 015–25 024, doi:10.1029/94JC01759.

Carter, D. J. T., P. G. Challenor, and M. A. Srokosz, 1992: An assessment of geosat wave height and wind speed measurements. *J. Geophys. Res.*, **97 (7)**, 11 383–11 392, doi:10.1029/92JC00465.

Challenor, P. G. and P. D. Cotton, 1999: Trends in TOPEX Significant Wave Height Measurement. Report, Southampton Oceanography Centre, Southhampton, UK.

Chelton, D. B. and P. J. McCabe, 1985: A Review of Satellite Altimeter Measurement of Sea Surface Wind Speed: With a Proposed New Algorithm. *J. Geophys. Res.*, **90 (3)**, 4707–4720, doi:10.1029/JC090iC03p04707.

Chelton, D. B., J. C. Ries, B. J. Haines, L.-L. Fu, and P. S. Callahan, 2001: Satellite Altimetry. *Satellite Altimetry and Earth Sciences: A Handbook of Techniques and Applications*, Academic Press, chap. 1, 1–131.

Chelton, D. D. and F. J. Wentz, 1986: Further development of an improved altimeter wind speed algorithm. *J. Geophys. Res.*, **91 (12)**, 14 250–14 260, doi:10.1029/JC091iC12p14250.

Cheney, R. E., B. C. Douglas, R. W. Agreen, L. Miller, D. L. Porter, and N. Doyle, 1987: *GEOSAT Altimeter Geophysical Data Record: User Handbook*. Rockville, NOAA.

Cotton, P. D. and D. J. T. Carter, 1994: Cross calibration of TOPEX, ERS-1, and Geosat wave heights. *J. Geophys. Res.*, **99 (12)**, 25 025–25 033, doi:10.1029/94JC02131.

Dobson, E., F. Monaldo, J. Goldhirsh, and J. Wilkerson, 1987: Validation of Geosat altimeter-derived wind speeds and significant wave heights using buoy data. *J. Geophys. Res.*, **92 (10)**, 10 719–10 731, doi:10.1029/JC092iC10p10719.

Donelan, M. A., 1990: Air-Sea Interaction. *The Sea: Ocean Engineering Science*, John Wiley & Sons, 239–292.

Dorandeu, J., 1999: *Side-B TOPEX Altimeter Evaluation.* CLS/DOS/NT Report 99.175, available online at http://www-aviso.cnes.fr:8090/HTML/information/missions/topex/topex_b_uk.html.

Evans, D., C. L. Conrad, and F. M. Paul, 2003: Handbook of Automated Data Quality Control Checks and Procedures of the National Data Buoy Center. Technical Document 03-02, NOAA National Data Buoy Center.

Freilich, M. H. and P. G. Challenor, 1994: A new approach for determining fully emperical altimeter wind speed model functions. *J. Geophys. Res.*, **99 (12)**, 25 051–25 062, doi:10.1029/94JC01996.

Glazman, R. E. and A. Greysukh, 1993: Satellite Altimeter Measurements of Surface Wind. *J. Geophys. Res.*, **98 (2)**, 2475–2483, doi:10.1029/92JC02659.

Goldhirsh, J. and E. Dobson, 1985: A recommended algorithm for the determination of ocean surface wind speed using a satellite-borne radar altimeter. Report JHU/APL SIR-85-U005, Applied Physics Laboratory, Johns Hopkins University, Laurel, MD.

Gourrion, J., D. Vandemark, S. Bailey, B. Chapron, G. P. Gommenginger, P. G. Challenor, and M. A. Srokosz, 2002: A Two-Parameter Wind Speed Algorithm for Ku-Band Altimeters. *J. Atmos. Ocean. Tech.*, **19 (12)**, 2030–2048.

Gower, J. F. R., 1996: Intercalibration of wave and wind data from TOPEX/POSEIDON and moored buoys off the west coast of Canada. *J. Geophys. Res.*, **101 (2)**, 3817–3829, doi:10.1029/95JC03281.

Hamilton, G. D., 1986: National Data Buoy Center Programs. *Bull. Am. Meteorol. Soc.*, **67 (4)**, 411–415.

Holthuijsen, L. H., 2007: *Waves in Oceanic and Coastal Waters*. Cambridge University Press, 387 pp.

Kshatriya, J., A. Sarkar, and R. Kumar, 2001: Comparison of TOPEX/POSEIDON Altimeter Derived Wind Speed and Wave Parameters with Ocean Buoy Data in the North Indian Ocean. *Mar. Geodes.*, **24 (3)**, 131–138.

Meindl, E. A. and G. D. Hamilton, 1992: Programs of the National Data Buoy Center. *Bull. Am. Meteorol. Soc.*, **73 (7)**, 985–993.

Monaldo, F., 1988: Expected differences between buoy and radar altimeter estimates of wind speed and significant wave height and their implications on buoy-altimeter comparisons. *J. Geophys. Res.*, **93 (3)**, 2285–2302, doi:10.1029/JC093iC03p02285.

Monaldo, F. and E. Dobson, 1989: On Using Signifficant Wave Height and Radar Cross Section to Improve Radar Altimeter Measurements of Wind Speed. *J. Geophys. Res.*, **94 (9)**, 12 699–12 701, doi:10.1029/JC094iC09p12699.

NDBC, cited 2008: *What are the sensors' reporting, sampling, and accuracy readings?* NOAA, National Data Buoy Center, available online at http://www.ndbc.noaa.gov/rsa.shtml.

NODC, cited 2008: *File format description for meteorology, oceanography, and wave spectra data from buoys (National Oceanographic Data Center F291* *format)*. NOAA, National Oceanographic Data Center, available online at http://www.nodc.noaa.gov/General/NODC-Archive/f291.html.

O'Leary, D. P., 1990: Robust Regression Computation Using Iteratively Reweighted Least Squares. *SIAM J. Matrix Anal. Appl.*, **11 (3)**, 466–480, doi:10.1137/0611032.

Queffeulou, P., 2003: Validation of ENVISAT RA-2 and JASON-1 altimeter wind and wave measurements. *IEEE Int.*, **5**, 2987–2989, doi:10.1109/IGARSS.2003.1294656.

Queffeulou, P., 2004: Long-Term Validation of Wave Height Measurements from Altimeters. *Mar. Geodes.*, **27 (3)**, 495–510, doi:10.1080/01490410490883478.

Queffeulou, P., A. Bentamy, and J. Guyader, 2004: Satellite Wave Height Validation Over the Mediterranean Sea. *Proceedings of the 2004 Envisat & ERS Symposium*.

Ray, R. D. and B. D. Beckley, 2003: Simultaneous Ocean Wave Measurements by the Jason and Topex Satellites, with Buoy and Model Comparisons. *Mar. Geodes.*, **26 (3)**, 367–382, doi:10.1080/714044527.

Stoffelen, A., 1998: Toward the true near-surface wind speed: Error modeling and calibration using triple collocation. *J. Geophys. Res.*, **103 (4)**, 7755–7766, doi:10.1029/97JC03180.

Tolman, H. L., 2002: Validation of WAVEWATCH III version 1.15. Tech. note omb 213, NOAA, Washington, DC. 37pp.

Trauth, M. H., 2007: *MATLAB Recipes for Earth Sciences*. 2d ed., Springer Verlag, 288 pp.

Walker, D. M., 1995: Measurement techniques and capabilities of the Geosat Follow-On

(GFO) radar altimeter. *Second Topical Symposium on Combined Optical-Microwave Earth and Atmosphere Sensing*, 226–228, doi:10.1109/COMEAS.1995.472314.

Witter, D. L. and D. B. Chelton, 1991: A Geosat Altimeter Wind Speed Algorithm and a Method for Altimeter Wind Speed Algorithm Development. *J. Geophys. Res.*, **96 (5)**, 8853–8860, doi:10.1029/91JC00414.

Young, I. R., 1993: An estimate of the Geosat altimeter wind speed algorithm at high wind speeds. *J. Geophys. Res.*, **98 (11)**, 20 275–20 285, doi:10.1029/93JC02117.

Young, I. R., 1999a: An intercomparison of GEOSAT, TOPEX and ERS1 measurements of wind speed and wave height. *Ocean. Eng.*, **26 (1)**, 67–81, doi:10.1016/S0029-8018(97)10016-6.

Young, I. R., 1999b: *Wind Generated Ocean Waves*. Elsevier Ocean Engineering Series, Elsevier Science, 306 pp., doi:10.1016/S0378-3839(00)00061-2.

Young, I. R. and G. J. Holland, 1996: *Atlas of the Oceans: Wind and Wave Climate*. 1st ed., Ocean Sciences Interactive Series (Elsevier), Pergamon, 241 pp.

List of Tables

TABLE 1. Summary of altimeter data products and characteristics including orbit parameters, name of data format and data source.

Satellite	Dates			Repeat Cycle	Inclination	Agency	Format	Source
ERS1	01 August 1991	–	10 December 1991	3 days	98.54°	ESA	CEOS	CD-ROM
	28 December 1991	–	30 March 1992	3 days		ESA	CEOS	
	14 April 1992	–	20 December 1993	35 days		ESA	CCSDS	
	23 December 1993	–	10 April 1994	3 days		ESA	CEOS	
	10 April 1994	–	26 September 1994	168 days		ESA	CEOS	
	28 September 1994	–	21 March 1995	168 days		ESA	CEOS	
	21 March 1995	–	17 May 1996	35 days		ESA	CCSD	
ERS2	21 April 1995	–	8 September 2008	35 days	98.54°	ESA	CCSD	CD-ROM
ENVISAT	24 September 2002	–	17 November 2008	35 days	98.54°	ESA	RA-2/MWR Level 2	CD-ROM
GEOSAT	30 March 1985	–	01 January 1990	17 days	108.00°	NOAA	JGM3-GDR	CD-ROM
GFO	07 January 2000	–	01 July 2008	17 days	108.04°	NOAA	GDR	Internet
JASON1	15 January 2002	–	03 May 2008	10 days	66.04°	NASA	PODAAC IGDR and GDR	Internet
TOPEX	22 September 1992	–	08 October 2005	10 days	66.04°	NASA	PODAAC MGDR-B	Internet

TABLE 2. Platform specific σ_o bias (i.e. the reported bias needs to be added to the satellite σ_o values) with related rms error ϵ for selected wind speed algorithms: Brown et al. (BR1981), Goldhirsh and Dobson (GD1985), Chelton and Wentz (CW1986), Witter and Chelton (WC1991), Freilich and Challenor (FC1994), Abdalla (A2007), and Gourrion et al. (GVC2002).

Altimeter	**BR1981**	**GD1985**	**CW1986**	**WC1991**	**FC1994**	**A2007**	**GVC2002**
ERS1	-0.205 dB	-0.264 dB	+0.095 dB	-0.039 dB	-0.177 dB	**+0.075 dB**	+0.578 dB
ϵ	1.32 m s^{-1}	1.23 m s^{-1}	1.41 m s^{-1}	1.20 m s^{-1}	1.26 m s^{-1}	**1.14 m s^{-1}**	1.18 m s^{-1}
ERS2	-0.154 dB	-0.241 dB	+0.093 dB	-0.045 dB	-0.209 dB	**+0.075 dB**	+0.512 dB
ϵ	1.32 m s^{-1}	1.27 m s^{-1}	1.62 m s^{-1}	1.34 m s^{-1}	1.45 m s^{-1}	**1.25 m s^{-1}**	1.29 m s^{-1}
ENVISAT	-0.363 dB	-0.431 dB	-0.114 dB	-0.268 dB	-0.424 dB	**-0.138 dB**	+0.299 dB
ϵ	1.31 m s^{-1}	1.26 m s^{-1}	1.56 m s^{-1}	1.33 m s^{-1}	1.39 m s^{-1}	**1.21 m s^{-1}**	1.27 m s^{-1}
GEOSAT	-0.060 dB	-0.053 dB	+0.160 dB	+0.087 dB	-0.073 dB	**+0.225 dB**	+0.595 dB
ϵ	1.71 m s^{-1}	1.68 m s^{-1}	1.96 m s^{-1}	1.80 m s^{-1}	1.91 m s^{-1}	**1.75 m s^{-1}**	1.98 m s^{-1}
GFO	-0.731 dB	-0.796 dB	-0.433 dB	-0.595 dB	-0.755 dB	**-0.481 dB**	-0.031 dB
ϵ	1.37 m s^{-1}	1.32 m s^{-1}	1.64 m s^{-1}	1.39 m s^{-1}	1.47 m s^{-1}	**1.28 m s^{-1}**	1.36 m s^{-1}
JASON1	-1.036 dB	-1.115 dB	-0.779 dB	-0.939 dB	-1.056 dB	**-0.789 dB**	-0.361 dB
ϵ	1.38 m s^{-1}	1.36 m s^{-1}	1.72 m s^{-1}	1.44 m s^{-1}	1.54 m s^{-1}	**1.33 m s^{-1}**	1.36 m s^{-1}
TOPEX	-0.752 dB	-0.837 dB	-0.469 dB	-0.627 dB	-0.777 dB	**-0.502 dB**	-0.108 dB
ϵ	1.27 m s^{-1}	1.21 m s^{-1}	1.49 m s^{-1}	1.21 m s^{-1}	1.32 m s^{-1}	**1.14 m s^{-1}**	1.16 m s^{-1}

Table 3. Overall calibration results using reduced major axis (RMA) regression. The analysis uses all available buoy-altimeter co-locations (n) for the full period of each altimeter mission. Also shown are results from earlier studies. Altimeter wind speed U_{10} was calculated from the Abdalla (2007) model and platform specific biases were applied (cf. Table 2).

		Zieger, Vinoth and Young (2009)						Queffeulou et al. (2004) for H_s Queffeulou (2003) for U_{10}				Young (1999a)		
	Altimeter	**slope**	**offset**	ϵ	**e**	ρ	**n**	**slope**	**offset**	ϵ	**n**	**slope**	**offset**	**n**
H_s	ENVISAT	1.069	-0.198	0.15 m	0.12 m	0.990	4 390	1.033	-0.183	0.19 m	1,280			
	ERS1	1.127	+0.280	0.20 m	0.16 m	0.984	2 079					1.243	+0.040	192
	ERS2	1.076	+0.042	0.17 m	0.13 m	0.989	7 885	1.064	+0.001	0.19 m	12,070			
	GEOSAT	1.076	+0.122	0.21 m	0.17 m	0.982	1 600					1.144	-0.148	203
	GFO	1.068	+0.102	0.15 m	0.12 m	0.991	6 179	1.080	+0.039		21,228			
	JASON1	1.036	+0.026	0.16 m	0.13 m	0.990	4 420	1.007	+0.039	0.19 m	2,853			
	TOPEX	1.049	-0.098	0.17 m	0.13 m	0.990	3 428	1.024	-0.048	0.17 m	7,826	1.067	-0.079	192
U_{10} (A2007)	ENVISAT	1.010	-0.110	1.11 m s^{-1}	0.86 m s^{-1}	0.941	2 926	0.964	+0.599	1.52 m s^{-1}	292			
	ERS1	1.047	-0.293	1.07 m s^{-1}	0.83 m s^{-1}	0.984	1 333					0.849	+1.217	192
	ERS2	1.005	-0.024	1.20 m s^{-1}	0.93 m s^{-1}	0.931	5 093							
	GEOSAT	1.015	-0.087	1.76 m s^{-1}	1.31 m s^{-1}	0.857	1 113					0.874	+0.337	196
	GFO	0.986	-0.059	1.31 m s^{-1}	1.02 m s^{-1}	0.925	4 136							
	JASON1	0.999	+0.070	1.28 m s^{-1}	0.99 m s^{-1}	0.936	2 865	0.986	+0.887	0.85 m s^{-1}	1,236			
	TOPEX	1.010	-0.062	1.11 m s^{-1}	0.87 m s^{-1}	0.948	2 486					0.943	+1.847	190

TABLE 4. Calibration results for all altimeters and periods over which the calibration is valid. Results are shown for both significant wave height (H_s) and 10 m wind speed (U_{10}), where the asterisk indicates the corrected value. Error statistics, rms error (ϵ), mean absolute error (e), correlation coefficient (ρ), the number of samples (n), rate of outliers, and the number of buoy stations used for the calibrations are shown.

	Altimeter	Scope	Calibration Function	ϵ	e	ρ	n	Outlier	Bouys
H_s	ENVISAT	24 September 2002 – 17 November 2008	$H_s^* = 1.069 \cdot H_s - 0.201$	0.156 m	0.118 m	0.990	4 506	2.6 %	87
	ERS1	01 August 1991 – 01 January 1994	$H_s^* = 1.122 \cdot H_s + 0.255$	0.193 m	0.148 m	0.985	1 005	1.7 %	58
	ERS1	01 January 1994 – 18 April 1995	$H_s^* = 1.150 \cdot H_s + 0.366$	0.215 m	0.169 m	0.986	510	1.0 %	58
	ERS1	18 April 1995 – 02 June 1996	$H_s^* = 1.102 \cdot H_s + 0.273$	0.177 m	0.135 m	0.988	595	2.2 %	58
	ERS2	29 April 1995 – 08 September 2008	$H_s^* = 1.076 \cdot H_s + 0.042$	0.172 m	0.132 m	0.989	8 060	2.2 %	87
	GEOSAT	31 March 1985 – 30 December 1989	$H_s^* = 1.076 \cdot H_s + 0.122$	0.216 m	0.166 m	0.982	1 638	2.3 %	42
	GFO	07 January 2000 – 01 July 2008	$H_s^* = 1.068 \cdot H_s + 0.102$	0.155 m	0.117 m	0.991	6 252	2.9 %	78
	JASON1	15 January 2002 – 03 May 2008	$H_s^* = 1.036 \cdot H_s + 0.026$	0.164 m	0.125 m	0.990	4 545	2.8 %	60
	TOPEX	25 September 1992 – 08 October 2005	$H_s^* = 1.050 \cdot H_s - 0.088$	0.162 m	0.124 m	0.991	3 510	2.5 %	45
U_{10} (A2007)	ENVISAT	24 September 2002 – 17 November 2008	$U_{10}^* = 1.010 \cdot U_{10} - 0.110$	1.097 m s^{-1}	0.860 m s^{-1}	0.941	2 979	1.8 %	87
	ERS1	01 August 1991 – 01 January 1994	$U_{10}^* = 1.066 \cdot U_{10} - 0.395$	1.056 m s^{-1}	0.827 m s^{-1}	0.944	653	1.7 %	58
	ERS1	01 January 1994 – 18 April 1995	$U_{10}^* = 1.025 \cdot U_{10} + 0.128$	1.056 m s^{-1}	0.800 m s^{-1}	0.946	328	2.1 %	58
	ERS1	18 April 1995 – 02 June 1996	$U_{10}^* = 1.046 \cdot U_{10} - 0.562$	1.040 m s^{-1}	0.807 m s^{-1}	0.952	377	1.3 %	58
	ERS2	29 April 1995 – 12 February 2000	$U_{10}^* = 1.043 \cdot U_{10} - 0.071$	1.114 m s^{-1}	0.862 m s^{-1}	0.939	1 693	2.1 %	87
	ERS2	12 February 2000 – 10 February 2001	$U_{10}^* = 0.980 \cdot U_{10} - 0.119$	1.102 m s^{-1}	0.884 m s^{-1}	0.936	331	0.0 %	87
	ERS2	10 February 2001 – 24 May 2005	$U_{10}^* = 0.972 \cdot U_{10} - 0.036$	1.162 m s^{-1}	0.914 m s^{-1}	0.934	1 832	1.7 %	87
	ERS2	24 May 2005 – 08 September 2008	$U_{10}^* = 1.041 \cdot U_{10} - 0.101$	1.214 m s^{-1}	0.959 m s^{-1}	0.931	1 312	1.2 %	87
	GEOSAT	31 April 1985 – 30 December 1989	$U_{10}^* = 1.015 \cdot U_{10} - 0.087$	1.706 m s^{-1}	1.306 m s^{-1}	0.857	1 166	4.5 %	42
	GFO	07 January 2000 – 21 December 2000	$U_{10}^* = 0.976 \cdot U_{10} - 0.623$	1.234 m s^{-1}	0.962 m s^{-1}	0.915	340	1.2 %	78
	GFO	21 December 2000 – 21 January 2007	$U_{10}^* = 1.015 \cdot U_{10} + 0.033$	1.099 m s^{-1}	0.853 m s^{-1}	0.949	3 283	2.1 %	78
	GFO	21 January 2007 – 01 July 2008	$U_{10}^* = 0.903 \cdot U_{10} - 0.489$	1.179 m s^{-1}	0.930 m s^{-1}	0.929	491	1.6 %	78
	JASON1	15 January 2002 – 03 May 2008	$U_{10}^* = 0.999 \cdot U_{10} + 0.070$	1.280 m s^{-1}	0.993 m s^{-1}	0.936	2 907	1.4 %	60
	TOPEX	22 September 1992 – 10 February 2001	$U_{10}^* = 0.991 \cdot U_{10} + 0.003$	1.079 m s^{-1}	0.851 m s^{-1}	0.945	1 243	1.7 %	45
	TOPEX	10 February 2001 – 21 October 2003	$U_{10}^* = 1.031 \cdot U_{10} - 0.140$	1.097 m s^{-1}	0.857 m s^{-1}	0.953	662	1.5 %	45
	TOPEX	21 October 2003 – 08 October 2005	$U_{10}^* = 1.018 \cdot U_{10} - 0.050$	1.130 m s^{-1}	0.877 m s^{-1}	0.949	620	1.6 %	45

List of Figures

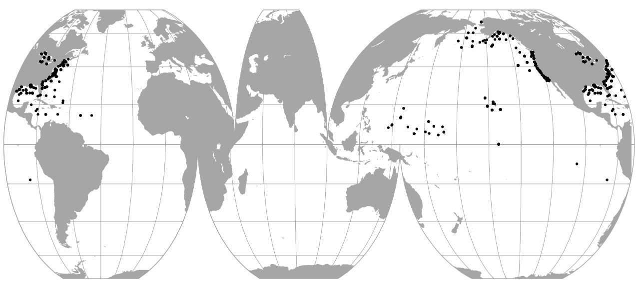

Fig. 1. Global distribution of all 195 NODC buoy stations distributed over 619 different locations based on a Mollweide interrupted equal-area projection. The spatial coverage is clearly limited to the Northern Hemisphere, whilst the temporal coverage features hourly records since 1985.

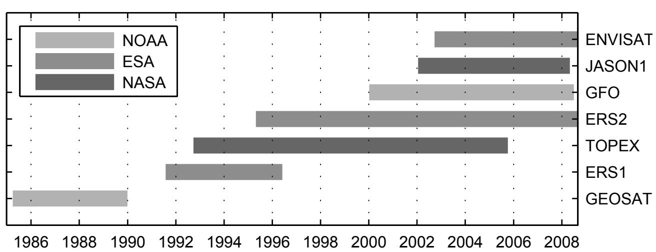

Fig. 2. Temporal coverage of available datasets of the previous seven altimeter missions.

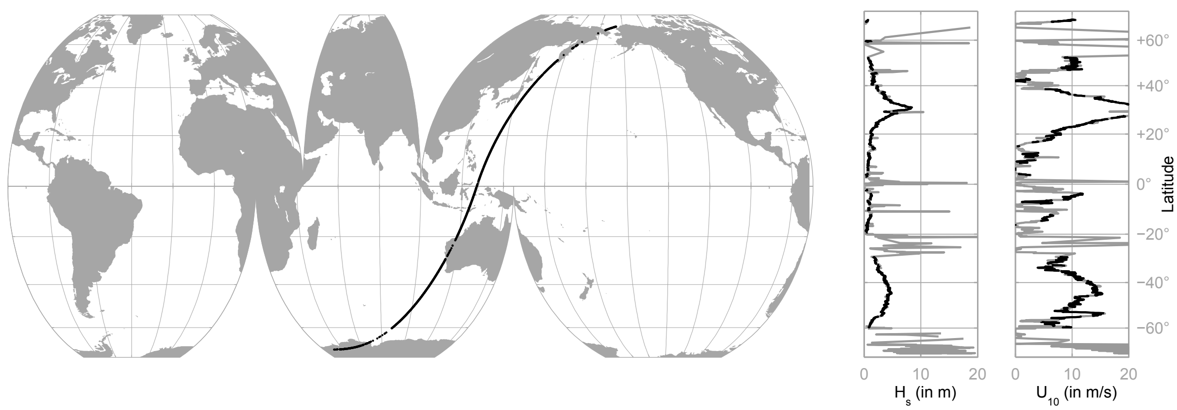

Fig. 3. Ascending GFO ground track recorded on 5 September 2007 (cycle 201, pass 34) commencing over the Antarctica and proceeding over the Southern Ocean, North Pacific Ocean towards the Arctic Ocean (left panel). The right panels show H_s and U_{10} as a function of latitude recorded along the ground track. Data errors ("spikes") are clearly evident in the data. This erroneous data (shown in gray) has been removed by the quality control process.

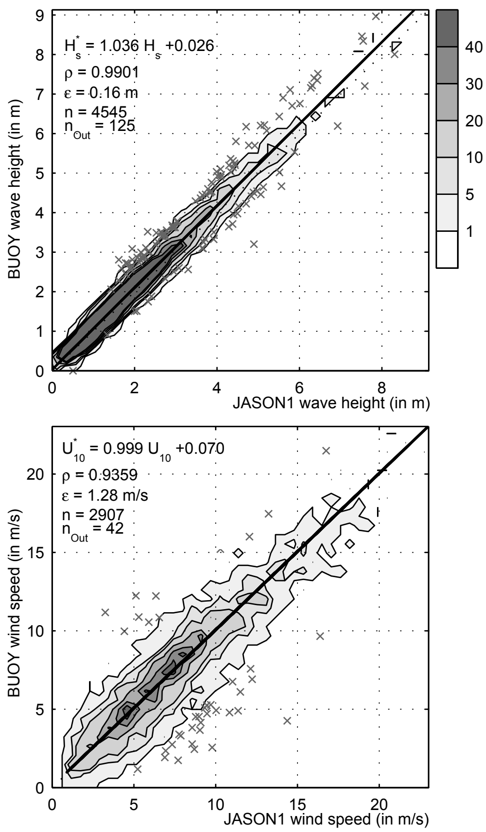

FIG. 4. Calibration results for JASON1 altimeter data. Shaded scatter density plot for significant wave height (upper) and wind speed (lower graph) of collocated measurements are shown. Collocated measurements are considered within 50 km radius and 30 min temporal separation. Error statistics for RMSE (ϵ), correlation coefficient (ρ), number (n) of sample point are given with outliers (n_{out}) labeled with crosses. The solid line represents the RMA fit. The axes were divided into 40 even increments and the contours show the number of data points in each increment square.

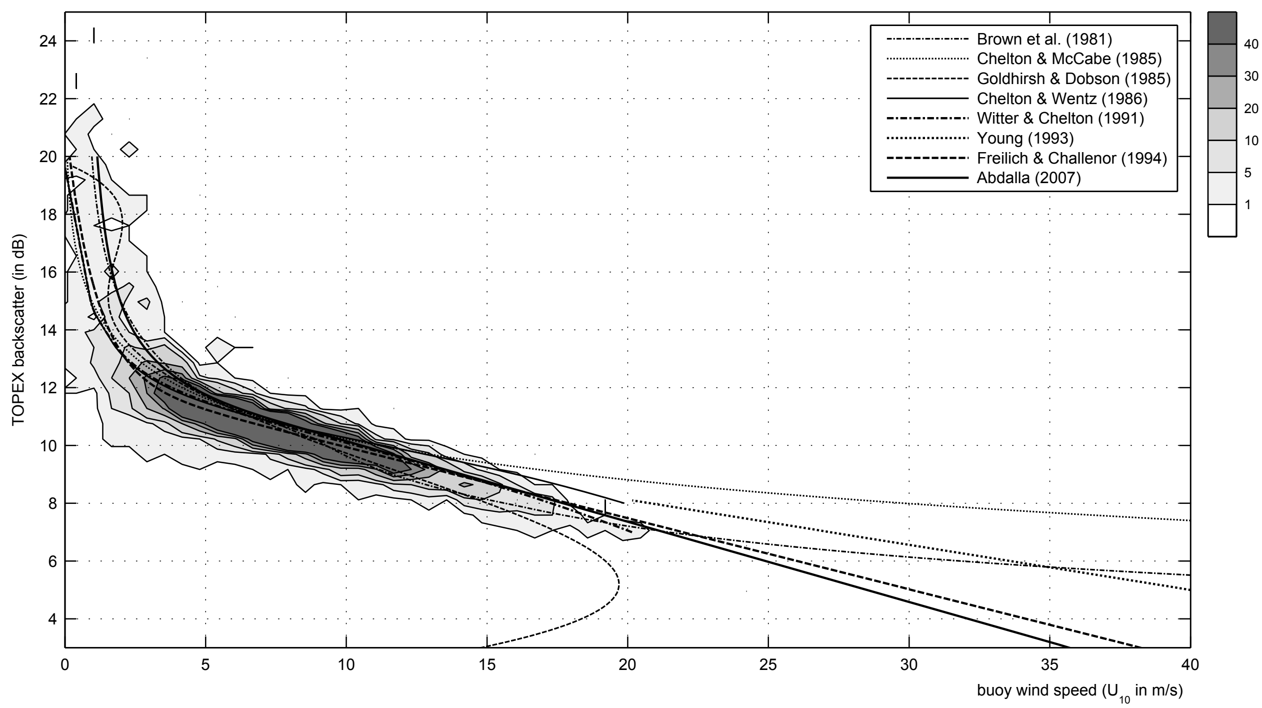

FIG. 5. Comparison of proposed wind speed algorithms for the estimation of wind speed, U_{10} from the altimeter radar backscatter (σ_o). The shaded contour plot shows isolines of data point density. The axes were each divided into 40 equally sized bins and the number of data points in each bin determined. Data is shown for TOPEX normalized radar cross section, σ_o adjusted by -0.502 dB. Note that with the exception of Young (1993), algorithms have been developed with data less than $U_{10} \approx 20\, m\, s^{-1}$. The results have been extrapolated beyond this value to show the effect of extrapolation to such wind speeds.

Fig. 6. Distribution of co-located measurements between JASON1 and ERS2 radar altimeters. During the latter part of the ERS2 mission an on-board storage failure limited the spatial coverage to the Northern Hemisphere. As a result, there is a greater density of co-location points in the North Atlantic and parts of the North Pacific.

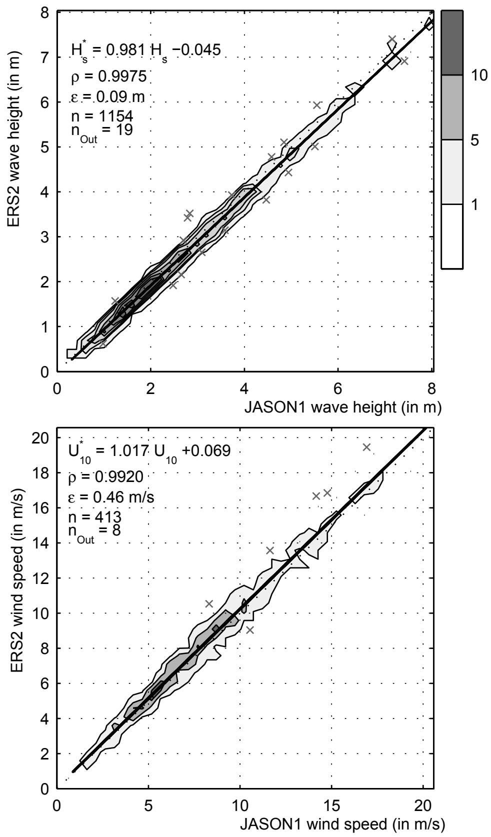

Fig. 7. Collocated measurements between JASON1 and ERS2 altimeters. Shaded scatter density plots show significant wave height (upper) and wind speed (lower graph). Contours are calculated as in Figure 4.

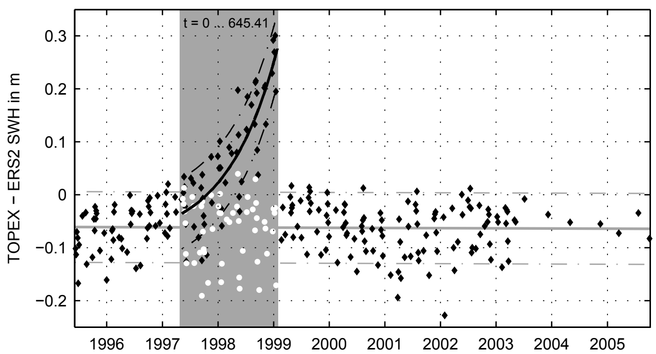

Fig. 8. Plot (20/1 block averages) illustrating differences in significant wave height between uncalibrated TOPEX and calibrated ERS2 measurements. The proposed drift correction $f(t)$ (Eq. (8)) with t in days was applied between 25 April 1997 and 30 January 1999, equivalent to cycles 170 to 235. Dash-dotted lines represent 1/2 standard deviation boundaries. The time period of the drift is shown by the shaded region. The white dots in this region shows the altimeter differences once the TOPEX drift has been removed using Eq. (8).

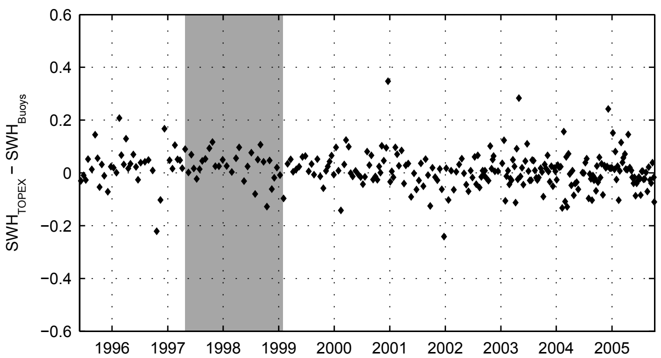

FIG. 9. Differences in H_s between TOPEX and buoy observations after applying the drift correction (Eq. (8)) and calibration function (cf. Table 4). The plot (block averaged at 12/1) covers the same time span as in Figure 8.

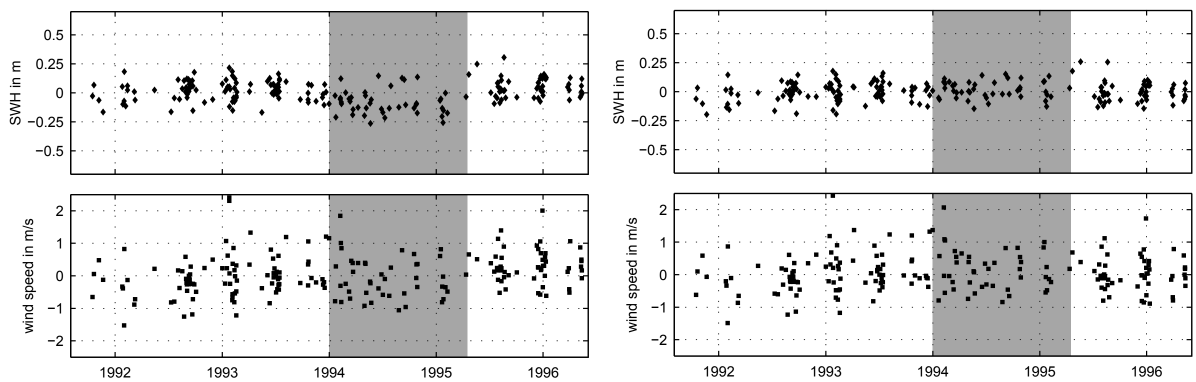

FIG. 10. Plot (block averaged at 12/1) showing differences between ERS1 and buoy H_s and U_{10}. The shaded region shows a time-dependent offset in H_s. The panels to the right show the differences once the partial RMA analysis was performed, removing the offset. Error statistics prior to the partial RMA analysis are: ϵ_{H_s}=0.20 m, $\epsilon_{U_{10}}$=1.11 m s^{-1}. The partial RMA analysis reduces these values to: ϵ_{H_s}=0.19 m and $\epsilon_{U_{10}}$=1.10 m s^{-1}.

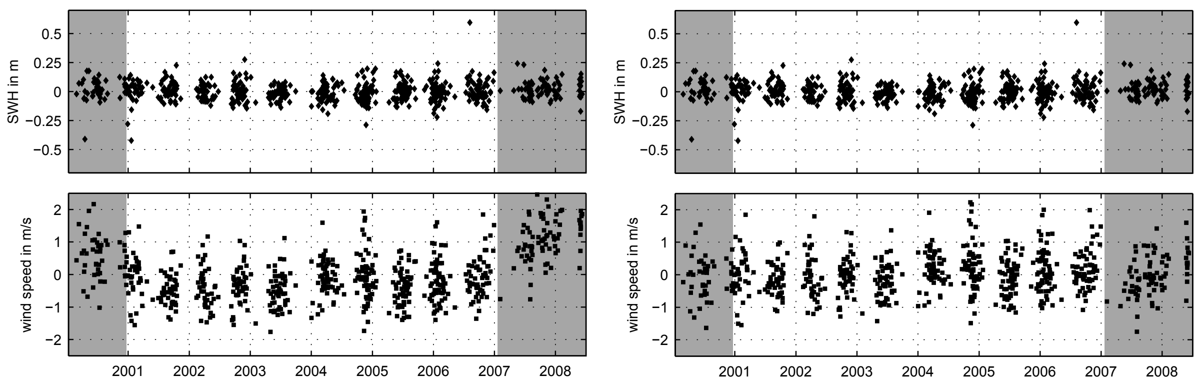

FIG. 11. Differences between GFO and buoy H_s and U_{10}. Deviations (shaded areas) in GFO wind speed measurements were successfully removed using the partial RMA calibration approach. Wind speed rms errors were improved from $\epsilon_{U_{10}}$=1.20 m s^{-1} (left) to $\epsilon_{U_{10}}$=1.18 m s^{-1} (right) while significant wave height was not altered ϵ_{H_s}=0.15 m.